FATIGUE DAMAGE IN NOTCHED GFR COMPOSITES WITH THERMAL AND DIGITAL IMAGE MEASUREMENTS

S. Giancane, F. W. Panella, V. Dattoma

Dipartimento di Ingegneria dell'Innovazione, Università del Salento, via per Monteroni, 73100, Lecce, ITALY, mail: simone.giancane@unile.it, francesco.panella@unile.it, vito.dattoma@unile.it.

Keywords: Damage, Fatigue, Digital Image Correlation, thermo-graphic analysis, Composites, Deformation, Hysteresis Energy, Compliance

Abstract

Complex time dependent damage phenomena are characteristic of Composites under fatigue; this is due to material structural heterogeneity and fibre/matrix interactions. Fatigue life is mainly determined by the progressive damage evolution, difficult to be modeled with numerical tools or mathematical frames. Experimental methods are to be applied to achieve correct information about the evolving fatigue damage and the authors propose a methodology based on Digital and Thermal Image analyses, to measure on notched GFRC specimens the dissipative sources in terms of temperature and deformation based data; starting from previous works, the measurements procedures were improved for these techniques, in order to obtain useful results with notched composites and capable to detect different damage states on specimen surface.

1 Introduction

The first observed damage mechanism in laminates is usually matrix cracks formation within off-axis plies and some engineering approximation exists to predict this crack formation because of continuous re-distribution of stress while life consumes [1-2].

A second important damage mode is due to the rupture of fibers of adjacent on-axis plies near the primary matrix crack tips, easy to be predicted for static loads. The third and most important type of damage is represented by local delamination in localized regions near the primary crack tips or between layers [3-5].

In every case, these events are accompanied by dissipation of energy, represented by the area of mechanical hysteresis loop, and produce a progressive decrease of laminate stiffness[6-7]. These measurements can sometimes show violent changing of the observed trend and the aim of this work is to correlate these observed phenomena with experimental methods. In fact, damage in composites is difficult to be modeled with numerical tools in a reliable way; important information could be omitted giving wrong results in terms of endurance expectancies. Therefore experimental methods are to be applied to achieve correct information about the evolving fatigue damage; the authors propose a methodology based on Digital and Thermal Image analyses to measure on notched GFRC specimens the dissipative sources in terms of temperature and deformation variations under fatigue; detecting energy dissipation during fatigue load and analyzing the notch tip and un-notched zones, in local way and subsequently in a full-field study.

The measurements procedures and data processing were improved for the Image Correlation and Thermographic techniques, in order to obtain useful results on notches. Shaped specimens with notches were fatigue tested under tensile load and the first and preliminary experimental results show the monitoring methods coherence with precise indications of the real damage.

2 Materials and experimental procedure

The material here studied is a E-glass/epoxy composite manufactured by vacuum bag molding technique obtaining a plate (uniform thickness of 4 mm) with a ply sequence of four quadriaxial fabric layers: [0 +45 90 -45] x 4 (see table 1 for properties of materials).
Notched specimens (figure 1) were obtained from a single plate by means of a milling machine with notch radius 2 mm; they were provided with opportune tabs according to standard ASTM D3039 [8], allowing an efficient load transmission during test and avoiding, at the same time, a damage of specimen caused by the grip system of test machine.

E-glass fibers	
Average value of Diameter (μm)	14
Young Modulus (MPa)	72500 GPa
Ultimate tensile strength (MPa)	2150 MPa
Strain to failure (%)	3.75
Epoxy Resin EC 15 + Hardening Additive W152 MLR (weight ratio 100:30) (ELANTAS)	
Density (g/ml)	1.08÷1.12
Young Modulus (MPa)	3100÷3500
Ultimate tensile strength (MPa)	68÷76
Strain to failure (%)	3.0÷8.0

Table 1. Mechanical properties of E-glass fibers and epoxy resin.

For this paper, few specimens were used; a preliminary static test and three fatigue experiments (table 2) were performed with an MTS hydraulic machine, load cells of 10 kN. During fatigue tests, executed with a tensile load ratio of 0.1, CCD camera and thermo-camera apparatus were used to register respectively 8-bit images and thermal maps of damage (Fig. 2a). On specimen surface, two defined regions are chosen for the needed measurements, as displayed in Fig. 2b.

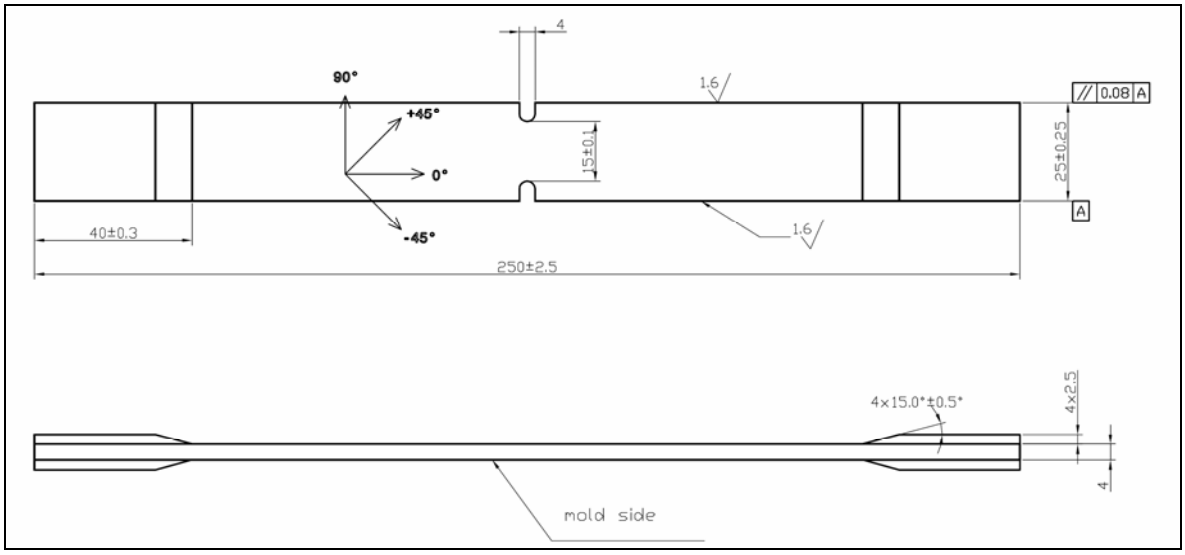

Figure 1. Geometry of the notched GFRP specimens.

Because of the necessity to reduce the time for data elaboration, it is preferred to store images with a rate of 10 fps and apply non-phased sinusoidal load of 21 Hz for fatigue tests. The choice of these values allowed a complete reconstruction of signal for the whole cycle in spite of under-sampling conditions, as reported in Figure 3. The MTS data were also stored with a frequency of 1000 Hz and the devices were triggered to synchronize the load signal and the acquisition processes.

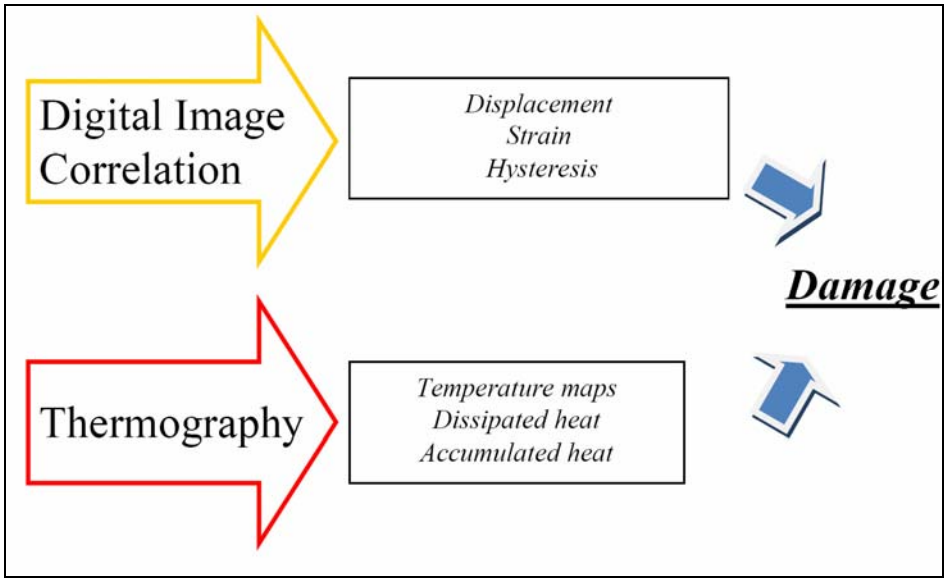

Figure 2a. Parallel damage detection through DIC (for the region in yellow square) and Thermography (region in red square) measurements.

In each test, two regions around the notch were observed with DIC and Thermography full-field analysis (Fig. 2b) at the notch tip and the evolution of damage was calculated and compared also in local way for three points in the proximity of notched section, where the main damage processes are expected to take place for concentration effects.

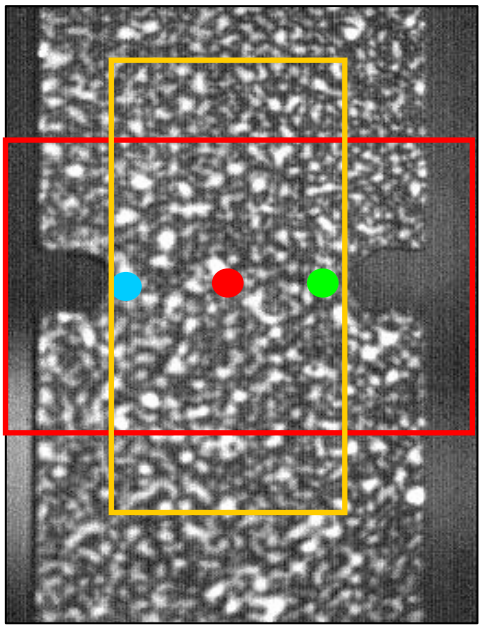

Figure 2b. The notched specimen processed area, Digital Image Correlation for the region in yellow and Thermography in the red region; the three points (cyan, red and green) where specific points for local damage evaluation.

Temperature maps were acquired by means of a FLIR 7500M camera (NETD=25 mK, image resolution of 320x256 pixel^2 , accuracy=±1%). Fatigue loads and cycle to failure are selected for short time tests in this paper for initial investigations, as showed in Tab. 2 and the damage phenomena takes place before 10.000 cycles. This way thermal processes are enhanced and initial correlation of damage in composites with thermal changes under fatigue can be analyses.

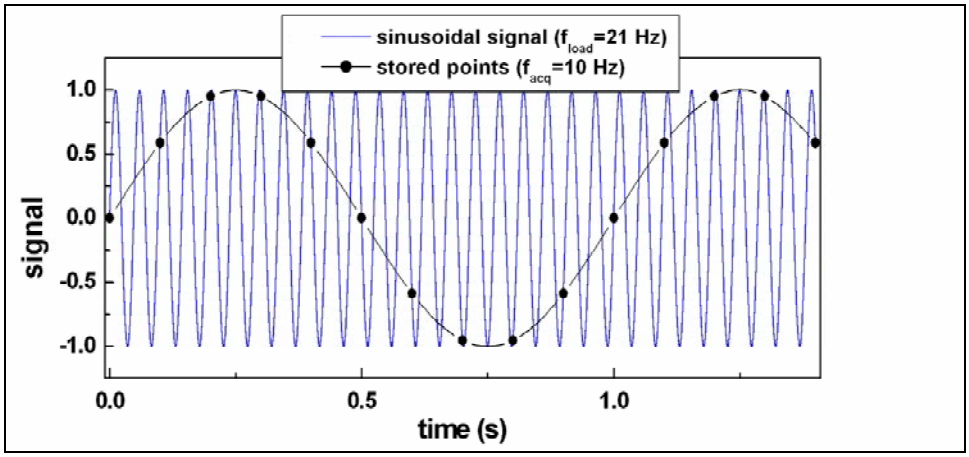

Figure 3. Acquired images with f_{acq} = 10 Hz for a sinusoidal load signal to be reconstructed at f_{load} = 21 Hz.

The precise temperature analysis of composite subjected to internal fatigue defects is well established (9-10), even that a standard procedure for thermo-graphic inspection is still not available, mainly because of different results and measurements procedure used by researchers. Despite this, the authors believe fatigue failure can be predicted analyzing composites with thermal methods under service. The main parameters to be measured is simply the local temperature at surface or indirect indicators, such as heat dissipation [4,11]. In case damage takes place immediately underneath the focal point, the dissipative heat during cyclic load can be easily detected and correlated to residual life.

Test ID	F_{alt} *(kN)*	F_{mean} *(kN)*	*Cycle to failure*
ES-A-3	4.63	5.66	*6678*
ES-A-4	4.35	5.31	*5111*
ES-A-5	4.04	4.93	*9495*
ES-A-1 Static test: F_{ult} = 13.8 kN			

Table 2. Scheme of performed tests.

3 Calibration and testing Set-up with Digital Image Analysis

Digital Image Correlation is based on pattern recognition and the correspondence between the sub-images associated to the markers of a virtual grid superimposed on the images [12,13]. Considering a number of images, the first is taken as reference and a virtual grid is superimposed on it; opportune correlation algorithms [16,17] allow to find the position of the markers of the deformed grid for every image (in terms of pixel) and to calculate the field of superficial displacements at the time, which an image as reference [14,15]; the authors produced few papers with this experimental technique. The images must present a significant contrast to make the process work, so the specimens were previously prepared painting them with white varnish spread on a black background (Fig. 4a).

. For all tests, images were stored with a spatial resolution of 0.145 mm/pixel by means of a DRS's Lighting RDT/1 high speed CCD camera with high frame rate.

Firstly, an evaluation of accuracy of displacement and strain measurements was performed employing a virtual image of the same specimen rigidly shifted of 1 pixel in horizontal direction. Correlation of the original and shifted images gave the results exposed in Figure 4. Displacements data are affected by a total dispersion of about 0.005 pixel in both direction (Fig. 4b) and we can assert that displacement measurements present a maximum error in the order of 10 μm. At the same time, the uncertainty in strain evaluation resulted to be about 1.6 10^{-4} in terms of pixels (Fig. 4c), giving rise to similar precision in terms of absolute strains.

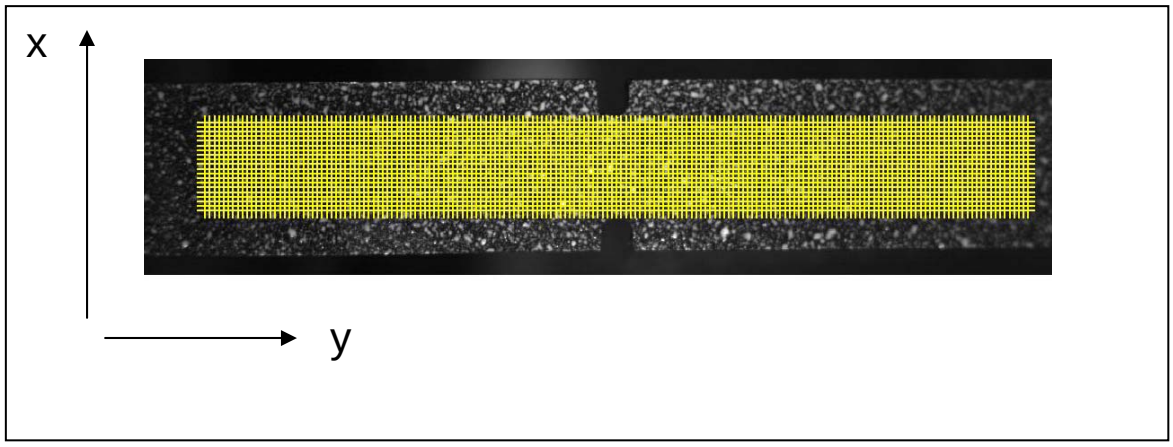

Figure 4a. Image of a notched specimen with a virtual superimposed grid.

In order to better apply the Digital correlation procedure, a Static test has been conducted on the specimen ES-A-1 and axial strains were calculated; five images per second were acquired and a speed of actuator of 1 mm/min was imposed. Averaging the values of ε_y for each loaded section on a data row (considering the specimen as mono-dimensional and identifying it with its axis) it is possible to follow the evolution of strain until the final failure occurrence (Fig. 5) at 13.8 kN, at frame 3000 . The first layer in front of the camera is an oriented –45° off axis layer and the strain calculated for the area close to the notches shows a strongly not linear behavior and elevated stress concentration. Rupture is mainly due to fibers separations from the laminate between layers, right beside the notch tip and small delaminatio is observed between the first layers in the notched region.

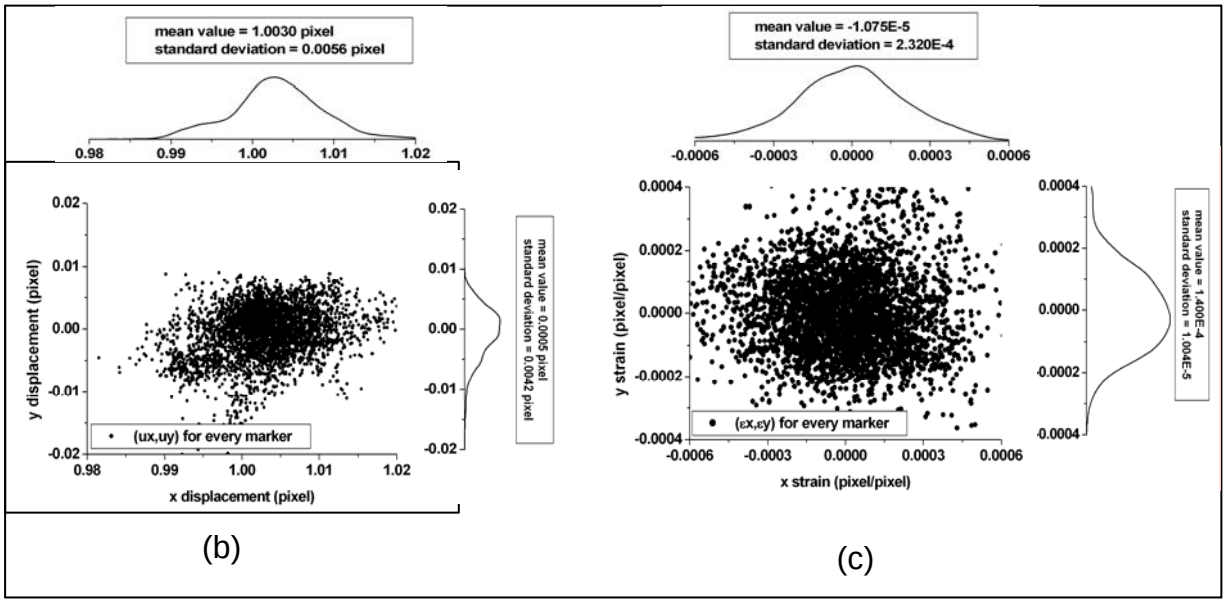

Figure 4b. Results of detected displacement points (b) and strains (c), as calculated between two images shifted of 1 pixel in x-direction.

It can be easily observed how the strain field is computed in uniform way along the specimen. Since the concentration factor is eliminated by using an average strain over each section, but a consistent damage state appears after 1500 images and progressively produces higher strains only in the zone where failure occurs.

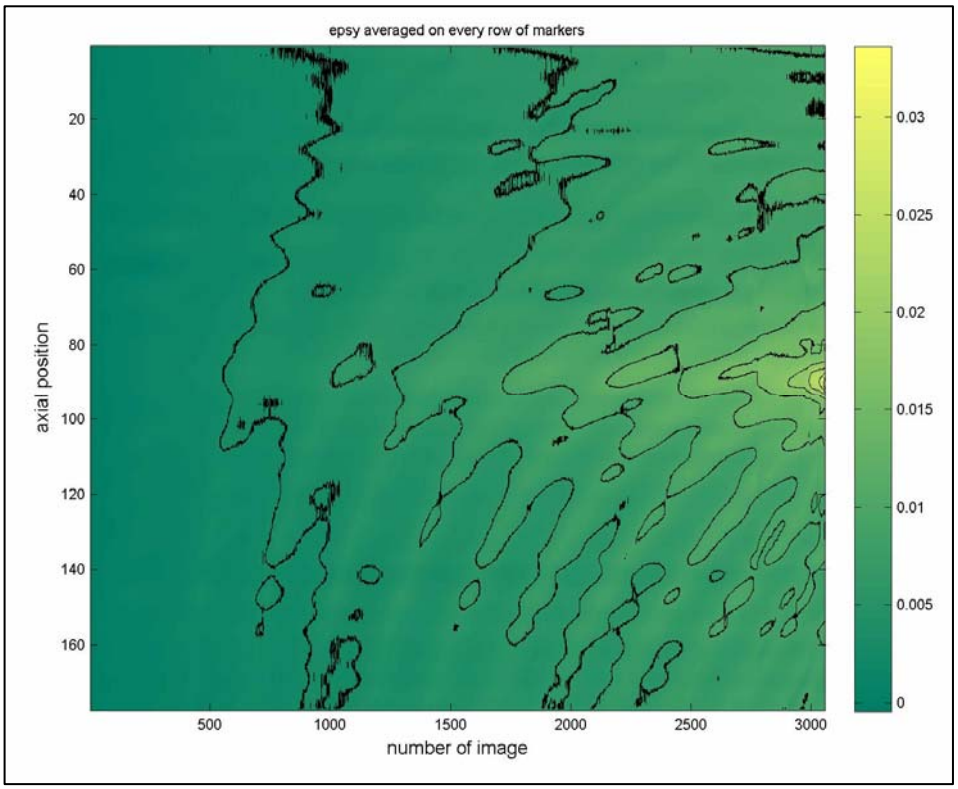

Figure 5. Static test results on ES-A-1 specimen map; ε_y are averaged on every row, image per image.

4 Thermo-graphic damage state analysis

During a fatigue test a specimen exchanges energy according to a general balance that can be stated as follows:

$$H = Q_{accumulated} + Q_{dissipated} + E_{damage} \quad (1)$$

where the terms in equation (1) are:

- H: mechanical hysteresis area (calculated from a σ-ε diagram) and representing the amount of energy supplied by test machine to specimen cycle by cycle; it can be calculated considering $\sigma = F/Section$ and calculating the strain value at each single marker of the grid, using DIC measurements. The base hypothesis is that the strain measured on the surface directed to camera is valid through the thickness of specimen.
- $Q_{accumulated}$: heat accumulated into the specimen and calculated as $\rho c \partial T/\partial t$ (where ρ is the density (1693 Kg/m^3), c thermal capacity (1547 J/kgK) and T the superficial temperature, measured with thermo-camera).
- $Q_{dissipated}$: heat dissipated by convection (dissipation for conduction and radiation is here neglected) according to the formula:

$$Q_{dissipated} = \left[h\left(T_s - T_a\right) + e\beta\left(T_s^4 - T_a^4\right)\right]\frac{A_{surf}}{V} \quad [2]$$

where T_s is the punctual temperature of the specimen surface, T_a is the air temperature (293 K), the emissivity e=0.85, the Stefan-Boltzman constant β=5.67*10^{-8} W/m^{2}K^4, the coefficient h defined as:

$$h = 1.42\left(\frac{T_s - T_a}{L}\right)^{0.25} \quad [3]$$

and A_{surf} , V and L respectively are the area, length and volume of the portion of specimen considered for calculation.

- E_{damage} : energy absorbed for nucleation of defects, their propagation and general evolution of fatigue failure.

Since H, Q_d and Q_a can be calculated on a portion of specimen, integrating the local hysteresis energy per unit volume and the Q values are estimated from temperature measurements, the balance equation 1 can be studied over time to determine the influence of each parameter and evaluate the real E_{damage} value by difference.
In order to perform this operation, we consider as significant example the fatigue test on specimen ES-A-3. The registered temperature and heat maps are reported in figures 6, where it can be observed that the main damage phenomena interests the left side of the notched section, bringing the specimen to its final failure. In fact, in that region temperatures are higher since the very first cycles, as well as the accumulated and dissipated heat are immediately increased; moreover, it can be observed how, in correspondence with the end of its life, the specimen exhibits a 45° tilted line where heat significantly accumulates and during final failure a cleavage effect occurs that direction.
More precisely, the Q_a value is observed to be more constantly distributed, probably because temperature variation in time are similar in the notched and un-notched region; on the other hand, the Q_d value assumes clearly higher result in the notch on the left, given that the damage state in that volume produces higher energy and therefore more dissipation with environment. This value seems to be a good indicator of damage severity.

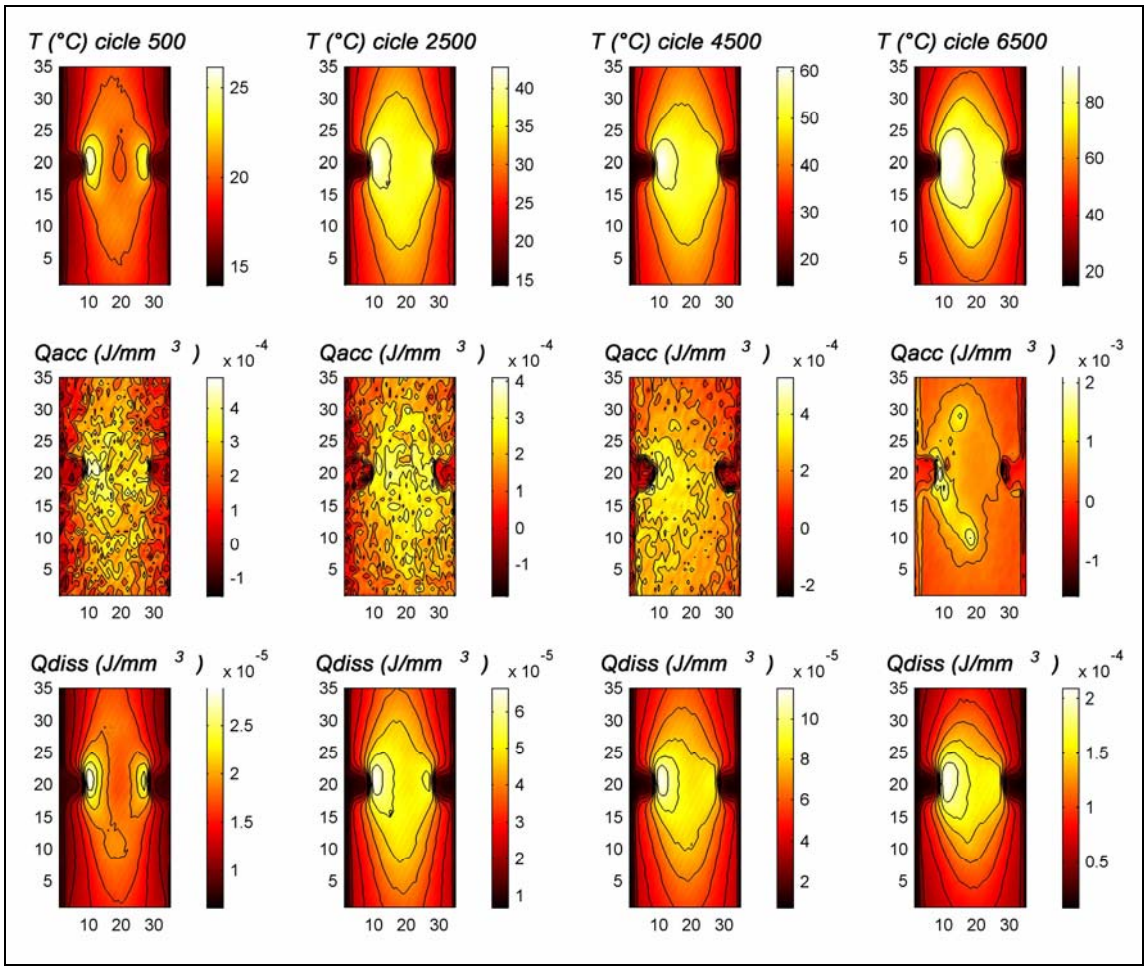

Figure 6. 2D maps of temperature, accumulated heat and dissipated heat for ES-A-3 specimen.

In Fig. 7 instead, 2D maps of volumetric hysteresis H on the monitored area for ES-A-3 specimen are reported in four different moments (from initial cycles up to fatigue failure), calculated locally on the base of strain DIC measurements and assuming proportional stresses. In the initial phase, the H value is extremely low and characterized by scatter, due to natural errors produced by the strain correlation algorytms and by the discreet pixel array of measurement points. Successively, when the stable damage takes place all over the specimen, a small progressive and uniform increase of H value is observed, probably originated by the decay properties of the laminate in the matrix. Finally, local rise of Hysteresis energy occurs at the notch, especially in the left side, up to failure.
Although the general behavior of Q and H parameters seems the same, producing the expected higher values in the same point at the left notch when catastrophic failure is near to happen, it is interesting to analyze these parameter well before the final rupture initiates and try to detect some kind of relevant changes or differences among them, helpful to predict the failure point location.

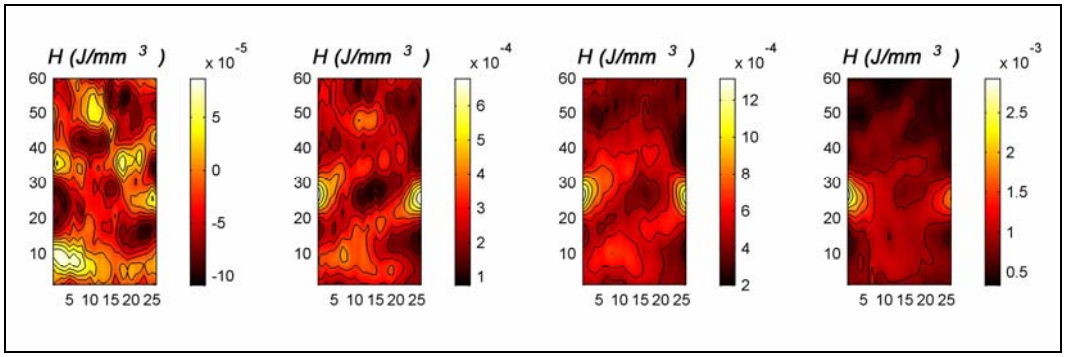

Figure 7. 2D maps of hysteresis area for ES-A-3 specimen.

5 Discussions of final results

At the moment we can investigate on the H and Q parameters interactions only for the 3 reference point during the cycling load, previously identified in Fig. 2b. The results can be used to calculate the damage energy E_d as reported in equation [1] for each point. Three curves (one for each point) can be traced to evaluate how damage differently evolves during fatigue life of the same specimen in the notched section (results are displayed in Fig. 8).

The central point shows a lower damage while the right one and in particular the left one are interested by a constant increasing of damage energy and in the final part of life (at about at 90 %) when damage energy has a violent rise as a mark of intense damage process.

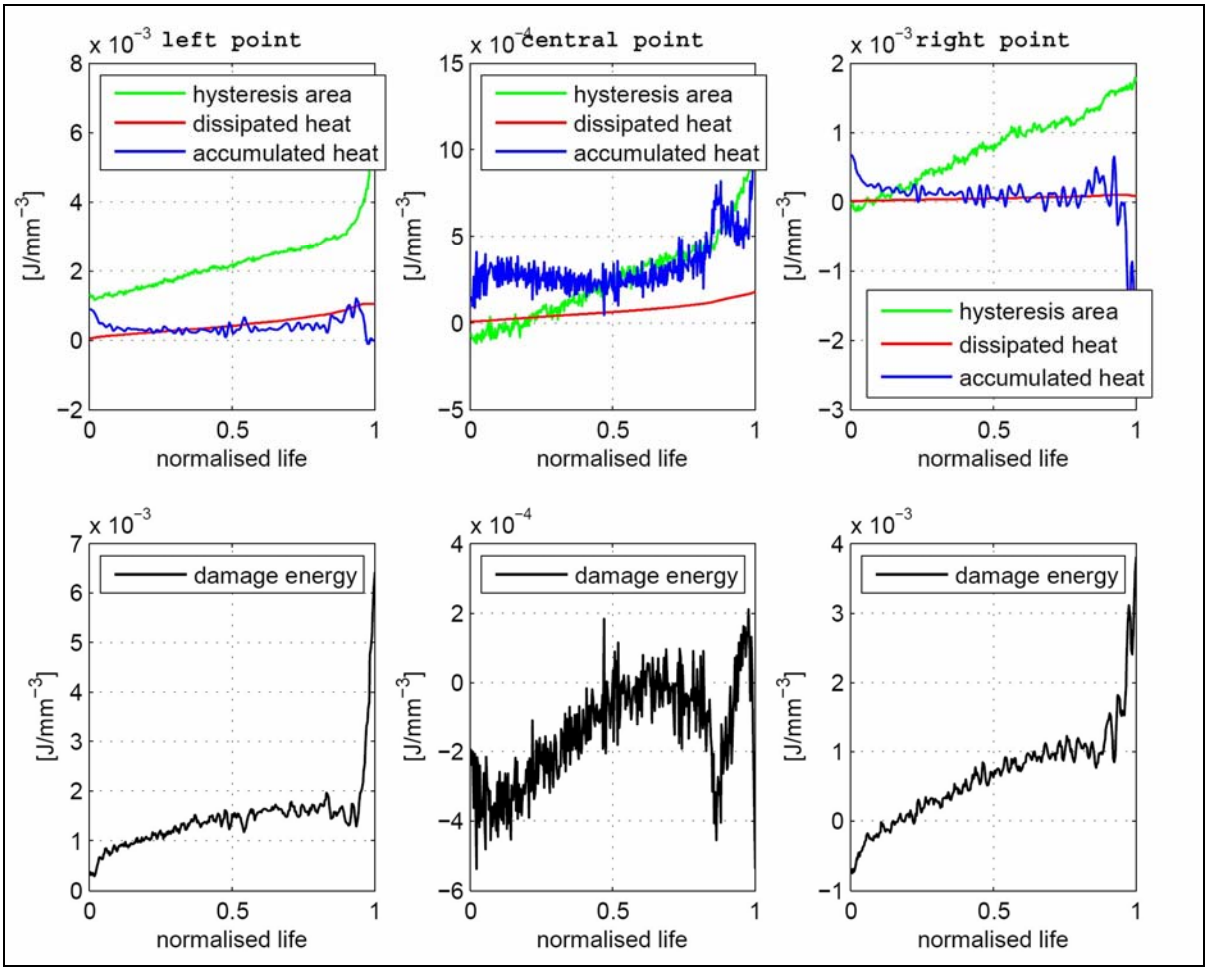

Figure 8. Energy balance and damage energy for the three points of notched section of specimen ES-A-3.

It is important to highlight a crucial aspect of the methodology here proposed: the dissipated and accumulated heat are calculated starting from temperature measurements, while hysteresis energy is related to strain maps and these quantities not only show coherence in terms of order of magnitude, but give evidence of the progressive damage. The use of notched specimens made possible to focus on the section where failure is expected to initiate and to catch the difference between critical zone (point 1 and 3) and non critical zone (point 3).

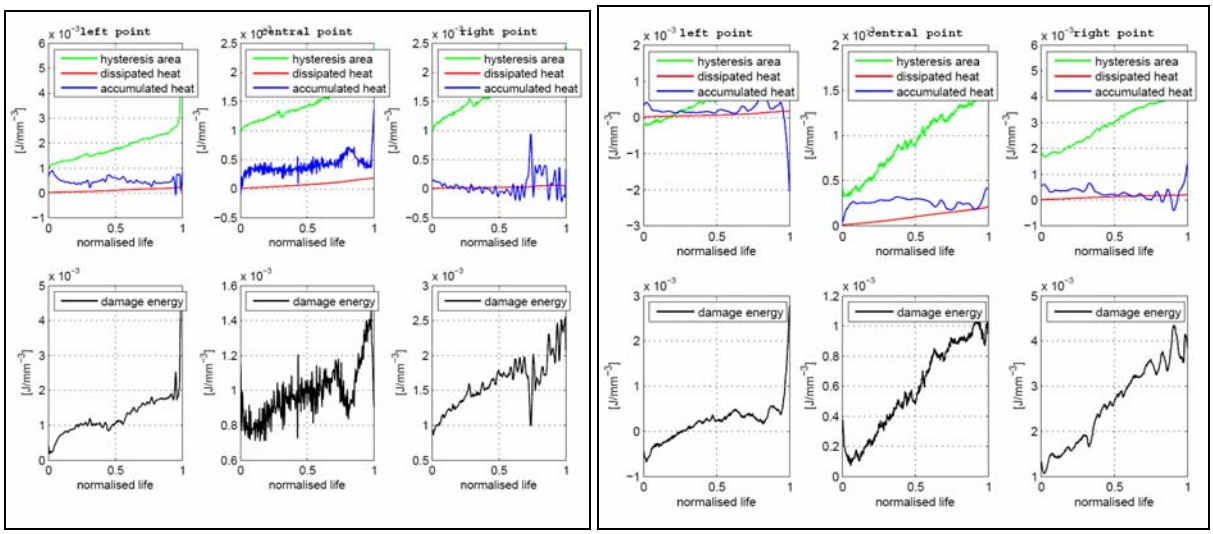

Figure 9. Energy balance and damage energy for the three points of notched section of specimen ES-A-4 and ES-A-5.

Similar considerations can be done for the other two tests (Figure 9). Also in these cases, the central points are less interested by damage than the point close to notch, as it could be expected.

The load frequency here used is quite high for a composite material, around 10 Hz and this caused an important temperature rise making at the same time negligible or less significant the dissipation terms if compared with hysteresis energies and accumulated heat, allowing to highlight the damage energy released during lifetime.

Conclusions

2D Digital Image Correlation technique and thermography were employed for the study of damage into composite notched specimens. A thermodynamic frame was chosen and the measures were elaborated to evaluate the damage evolution in three points in the notched section, for the whole duration of each test.

The results show coherence and reliability and allow to precisely define the damage energy. Next activity will be focused on the possibility to evaluate the damage maps and not only the punctual value in some position, in order to employ this encouraging approach on different components and define an automatic procedure to characterize damage on the whole surface for the definition of correct residual life.

References

1. O'Brein T. K., "Damage in Composite Materials: Basic Mechanism Accumulation, Tolerance, and Charaterization". *ASTM STP 775*, K. L. Reifsnider Ed., PA, Philadelphia, 1982, pp. 140-168.

2. Reifsnider K L., "Damage and Damage Mechanics". *Fatigue of Composite Materials*, K. L. Reifsnider Ed., Elsevier Science Publisher B. V., 1990, pp. 11-77.

3. O'Brein T. K., Hooper S. J., "Local Delamination in Laminate with Angle Ply Matrix Cracks, Part I: Tension Test and Stress Analysis". *ASTM STP 1156*, W. W. Stinchcomb and N. E. Ashbaugh, Eds., Philadelphia, PA, 1993, pp. 491-506.
4. Giancane S., Dattoma V., Morabito A. E., Panella F. W., "Studio del Danneggiamento a Fatica di Laminati Compositi a Fibra Lunga". *XXXIV Convegno Nazionale AIAS 2005*, Politecnico di Milano, 14-17 Settembre 2005.
5. S. Giancane, F.W. Panella, V. Dattoma 'Characterization of fatigue damage in long fibre epoxy composite laminates' International Journal of Fatigue, Volume 32, Issue 1, January 2010, Pages 46-53.
6. Dalmas D., Laksimi A., "On the Method of Determination of Strain Energy Release Rate During Fatigue Delamination in Composite Materials". *Applied Composite Materials*, Vol.6, 327-340, 1999.
7. W. W, Bakis C. E., "Fatigue Behavior of Composite Laminates". *Fatigue of Composite Materials*, K. L. Reifsnider Ed., Elsevier Science Publisher B. V., 1990, pp. 105-180
8. ASTM - *Standard Test Method for Tensile Properties of Polymer Matrix Composite Materials* - Designation: D 3039/D 3039M-00 (Reapproved 2006)
9. S. Giancane, V. Dattoma, F. Palano, F.W. Panella 'Controllo non distruttivo su laminati gfrp mediante termografia pulsata' AIAS 2010 – XXXIV National Conference, 7-10 Settembre 2010, Maratea, Italia.
10. Steinberger, R.; Valadas Leitaao, T.I.; Ladstaatter, E.; Pinter, G.; Billinger, W.; Lang, R.W 'Infrared thermographic techniques for non-destructive damage characterization of carbon fibre reinforced polymers during tensile fatigue testing' *International Journal of Fatigue*, Volume 28, Issue 10, October 2006, Pages 1340-1347.
11. Gamstedet E., Redon O., Brondsted P. Fatigue dissipation and failure in unidirectional and angle-ply glass/fiber/carbon fiber hybrid laminates. *Key Engineering Materials*. 2002;221-222: 35-48.
12. Sutton S, Wolters MJ, Peters WH, Ranson WF, McNeill SR. Determination of displacements using an improved digital correlation method. *Image Vision Comput* 1983;1(3):133-139.
13. Kobayashi AS. *Handbook on experimental mechanics*. 2nd ed.. New York: Society for Experimental Mechanics; 1993
14. S. Giancane, F.W. Panella, R. Nobile, V. Dattoma 'Fatigue damage evolution of fiber reinforced composites with digital image correlation analysis' *Procedia Engineering,* Volume 2, 10th International Fatigue Congress, FATIGUE 2010; Prague – April 2010
15. P-L Reu, T.J. Miller, The application of high-speed digital image correlation, *J. Strain Alanysis*, 43 (2008), 673-688
16. Munteanu C. Evaluation of the sequential similarity detection algorithm applied to binary images. *Science B.V.* ; 1981.
17. Majumdar J, Dilip Y. Implementation of Image Registration Algorithms for Real-time Target Tracking Through Video Sequences. Aeronautical Development Establishment, Bangalore - 560 093. *Defence Science Journal* 2000;52(3): 227-242.
18. S. Giancane, F.W. Panella, V. Dattoma 'Characterization of fatigue damage in long fibre epoxy composite laminates' *International Journal of Fatigue*, Volume 32, Issue 1, January 2010, Pages 46-53
19. Stinchcomb W. W, Bakis C. E., "Fatigue Behavior of Composite Laminates". *Fatigue of Composite Materials*, K. L. Reifsnider Ed., Elsevier Science Publisher B. V., 1990, pp. 105-180
20. Gamstedet E., Redon O., Brondsted P. Fatigue dissipation and failure in unidirectional and angle-ply glass/fiber/carbon fiber hybrid laminates. *Key Engineering Materials*. 2002;221-222: 35-48.